JOURNAL OF PROPULSION AND POWER
Vol. 12, No. 4, July–August 1996

Numerical Flowfield Analysis of the Next Generation Vulcan Nozzle

G. Hagemann* and G. Krülle*
DLR, German Aerospace Research Establishment, D-74239 Hardthausen, Germany
and
K. Hannemann†
Institute for Fluid Mechanics, D-37073 Göttingen, Germany

For numerical simulations of reacting, viscous nozzle flows in advanced rocket nozzles, a numerical method has been developed. The code is based on the well-established DLR Euler/thin layer Navier–Stokes code NSHYP that was originally written for hypersonic re-entry flow simulations. The code solves the three-dimensional, time-dependent Euler and thin-layer Navier–Stokes equations in conservation-law form. Hydrogen and oxygen are considered as fuel and oxidizer, respectively. The passive scalar approach accounts for the multicomponent diffusion effects. Turbulent transport is described with an algebraic eddy–viscosity, and a k-ε two-equations model. Calculations of conventional bell nozzles were performed. Results of Vulcan Mark 1 nozzle flow simulations are shown and compared in detail with another well-established numerical approach, based on the method of characteristics. A modified Vulcan engine is proposed, where the gas generator exhaust gases are injected into the main nozzle. Results of an engine analysis are presented. Based on this engine analysis, numerical flowfield calculations of the modified nozzle were performed and are presented.

Nomenclature

c = mass fractions
D = diffusion coefficient
E, F, G = fluxes
e = absolute specific energy
F = thrust
h = specific enthalpy
I = specific impulse
k = turbulent kinetic energy
$\dot{m}$ = mass flow
p = pressure
q = conservative variables
R = specific gas constant
Re = Reynolds number
r = mass ratio oxidizer/fuel
r_{throat} = throat radius, Vulcan $r_{throat} = 0.1312$ m
S = diffusive flux
T = temperature
t = time
u, v, w = velocity components
x, y, z = Cartesian coordinates
ε = dissipation
ε_{ar} = area ratio
ε_r = emission coefficient
ε_s = internal, specific energy
κ = isentropic coefficient
λ = heat conductivity
μ = dynamic viscosity
ξ, η, ζ = transformed coordinates
ρ = density
τ = shear stress

Subscripts
c = combustion chamber
H_2^* = H_2 element
l = laminar
O_2^* = O_2 element
s = specific
t = turbulent
vac = vacuum

Introduction

THE reduction of Earth to orbit launch costs in conjunction with an increase in launcher reliability and operational efficiency are the key demands on future space transportation systems. This article discusses a potential gain in integral performance data that can be achieved with open-cycle engines, where turbine exhaust gases are dumped into the ambiance. Based on an existing engine concept, the European Vulcan engine, a modified version was designed by the authors. The only modification is the turbine exhaust gas injection into the main nozzle.

Flowfield calculations of this modified engine were performed to show the potential performance gain that can be achieved with the turbine exhaust gas injection.

Numerical Model

The fluid is assumed to be a viscous, reacting mixture of perfect gases.[1,2] Furthermore, thermal and chemical equilibrium of H_2–O_2 mixtures are assumed, since performance losses because of chemical nonequilibrium effects can be neglected in high-pressure rocket engines.[3]

The motion of this fluid is governed by the Navier–Stokes equations, including the conservation laws of the individual species. External forces and heat sources are not taken into account. In case of chemically reacting flows, species conservation equations must be solved for all species present in the fluid. Assuming constant mass diffusion coefficients for all species, the system of species conservation equations can be

Presented as Paper 95-2782 at the AIAA/ASME/SAE/ASEE 31st Joint Propulsion Conference and Exhibit, San Diego, CA, July 10–12, 1995; received Aug. 28, 1995; revision received Dec. 9, 1995; accepted for publication March 18, 1996.

*Aerospace Engineer, Lampoldshausen Research Center.
†Aerospace Engineer, Göttingen Research Center.

reduced. Here, only two equations for element mass conservation of hydrogen (H_2) and oxygen (O_2), respectively, have to be solved. The complete three-dimensional, unsteady, compressible Navier–Stokes equations can be written as

$$\frac{\partial \boldsymbol{q}}{\partial t} + \frac{\partial \boldsymbol{E}}{\partial x} + \frac{\partial \boldsymbol{F}}{\partial y} + \frac{\partial \boldsymbol{G}}{\partial z} = \frac{\partial \boldsymbol{E}_v}{\partial x} + \frac{\partial \boldsymbol{F}_v}{\partial y} + \frac{\partial \boldsymbol{G}_v}{\partial z} \tag{1}$$

with the vector of the conserved variables $\boldsymbol{q}$ and the convective fluxes

$$\boldsymbol{q} = \begin{bmatrix} \rho_{O_2^*} \\ \rho_{H_2^*} \\ \rho u \\ \rho v \\ \rho w \\ e \end{bmatrix}, \quad \boldsymbol{E} = \begin{bmatrix} \rho_{O_2^*} u \\ \rho_{H_2^*} u \\ \rho u^2 + p \\ \rho uv \\ \rho uw \\ (e + p)u \end{bmatrix}$$

$$\boldsymbol{F} = \begin{bmatrix} \rho_{O_2^*} v \\ \rho_{H_2^*} v \\ \rho vu \\ \rho v^2 + p \\ \rho vw \\ (e + p)v \end{bmatrix}, \quad \boldsymbol{G} = \begin{bmatrix} \rho_{O_2^*} w \\ \rho_{H_2^*} w \\ \rho wu \\ \rho wv \\ \rho w^2 + p \\ (e + p)w \end{bmatrix}$$

and the viscous fluxes $\boldsymbol{E}_v$, $\boldsymbol{F}_v$, and $\boldsymbol{G}_v$

$$\boldsymbol{E}_v = \begin{bmatrix} (\rho D)\left(\dfrac{\partial c_{O_2^*}}{\partial x}\right) \\ (\rho D)\left(\dfrac{\partial c_{H_2^*}}{\partial x}\right) \\ \tau_{xx} \\ \tau_{yx} \\ \tau_{zx} \\ u\tau_{xx} + v\tau_{yx} + w\tau_{zx} + \lambda \dfrac{\partial T}{\partial x} + (\rho D) \displaystyle\sum_{i=1}^{6} \left(h_i \frac{\partial c_i}{\partial x}\right) \end{bmatrix}$$

Because of the similarity of $\boldsymbol{E}_v$, $\boldsymbol{F}_v$, and $\boldsymbol{G}_v$, only $\boldsymbol{E}_v$ is shown here.

At high Reynolds numbers it has been shown by an order of magnitude analysis[4] that viscous effects in streamwise and circumferential directions can be neglected. Additionally, grid spacings in these directions are, in general, so large that viscous effects cannot be resolved sufficiently. This simplification leads to the thin layer Navier–Stokes equations, which can be written in nondimensional, conservation-law form for generalized curvilinear coordinate systems as

$$\frac{\partial \hat{\boldsymbol{q}}}{\partial t} + \frac{\partial \hat{\boldsymbol{E}}}{\partial \xi} + \frac{\partial \hat{\boldsymbol{F}}}{\partial \eta} + \frac{\partial \hat{\boldsymbol{G}}}{\partial \zeta} = \frac{1}{Re_\infty} \frac{\partial \hat{\boldsymbol{S}}}{\partial \zeta} \tag{2}$$

Here, $\hat{\boldsymbol{E}}$, $\hat{\boldsymbol{F}}$, and $\hat{\boldsymbol{G}}$ are the inviscid fluxes in the streamwise ξ, circumferential η, and wall normal direction ζ, respectively. The vector $\hat{\boldsymbol{S}}$ represents the viscous flux in the wall normal direction.

The time derivatives are approximated by the first-order Euler implicit formula. The spatial, inviscid fluxes are discretized in the form of the upwind Harten and Yee approximation,[1] which is a high-resolution, second-order, total variation diminishing (TVD) scheme. Viscous fluxes are discretized with second-order accuracy central differences.

Thermodynamic and Transport Properties

To complete the set of equations, further relations are needed to describe the thermodynamic and transport properties of the fluid.

The implementation of perfect or equilibrium gas equations of state requires the knowledge of pressure and temperature as a function of density and internal energy. The latter can be obtained from the conserved variables according to the relation:

$$\varepsilon_s = \frac{e}{\rho} - \frac{1}{2} \frac{(\rho u)^2 + (\rho v)^2 + (\rho w)^2}{\rho^2} \tag{3}$$

In the case of calorically perfect gases, the previous relations can be directly calculated from $\varepsilon_s = c_v T$ and $p = (\kappa - 1)\rho\varepsilon_s$. At temperatures above 800 K, the vibrational energy modes of molecules become excited, absorbing some energy that would usually transfer to the translational and rotational motion. Furthermore, chemical reactions, occurring at higher temperatures, absorb extra energy because of the dissociation of molecules. Therefore, temperature increase, e.g., from shocks, will be lower as predicted using the calorically or thermally perfect gas assumptions. For the simulation of high-pressure, H_2–O_2 rocket nozzles flows, these effects are reasonably simulated under the assumption of a local thermochemical equilibrium.[3] The following species are considered to be relevant for hydrogen/oxygen systems up to temperatures of 3600 K: H_2O, H_2, H, O_2, O, and OH. Temperature dependences of the equilibrium constants are taken from the literature. Internal energies and enthalpies of the individual species are calculated with relations of the statistical thermodynamic[5] in terms of partition functions.

The transport coefficients of the individual species are calculated with relations of the gas kinetic theory,[5] where intermolecular forces are described by the Lennard–Jones (6–12) potential.

The mixture transport coefficients for a multicomponent mixture are defined by means of the Wilke rule.[5] The diffusion coefficients follow from a constant Lewis number assumption for the case of $Le = 1$.

Turbulence

Turbulent transport is simulated with an algebraic eddy–viscosity model and with a k-ε two-equation model. The algebraic eddy–viscosity model is taken in a form of the Baldwin–Lomax model.[5]

The two-equation model is a low Reynolds number model that takes into account the damping effects of the nozzle walls.[5] This model requires a complete resolution of the boundary layer down to its laminar sublayer (wall-nearest grid point in the order of $y^+ = 0.1$). Dirichlet conditions for the velocities ($u = v = w = 0$) and the turbulence variables ($k = \varepsilon = 0$) are used. Turbulent coefficients of heat conductivity and diffusion are calculated under the assumption of a constant turbulent Prandtl and Lewis number ($Pr_t = 0.9$, and $Le_t = 1.0$).

Computational Results

Vulcan Mark 1 Nozzle

Calculations of the European Vulcan Mark 1 nozzle were performed. Results of these calculations are compared with corresponding data obtained by the NASA TDK program.[2] The plenum chamber parameters chosen for these calculations are given in Table 1. The basic design of the Vulcan Mark 1 engine is shown in Fig. 1, together with the finite difference mesh used for these simulations. Wall-nearest grid points are located at a normalized distance of $y^+ \approx 0.1$. Various finite difference meshes were chosen for the numerical simulations to study their influence and to ensure mesh-independent results on integral performance data, starting with 100 grid points in a streamwise direction and 35 grid points in a wall-normal direction.[8] Figures 2–4 show different flow parameter on the centerline and at the wall of the Vulcan nozzle. Additionally, TDK calculation data are included where chemical equilibrium

Table 1 Plenum chamber data Vulcan engine

	T_c, K	p_c, bar	O/F[a]
Vulcan	3538.0	102.0	6.0

[a]Oxidizer/fuel.

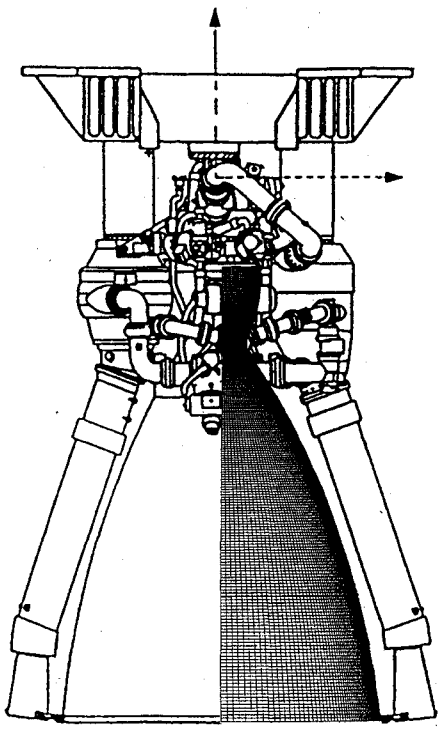

Fig. 1 Vulcan Mark 1 engine with finite difference mesh (number of grid points in streamwise, wall-normal, and circumferential direction 205 · 100 · 3).

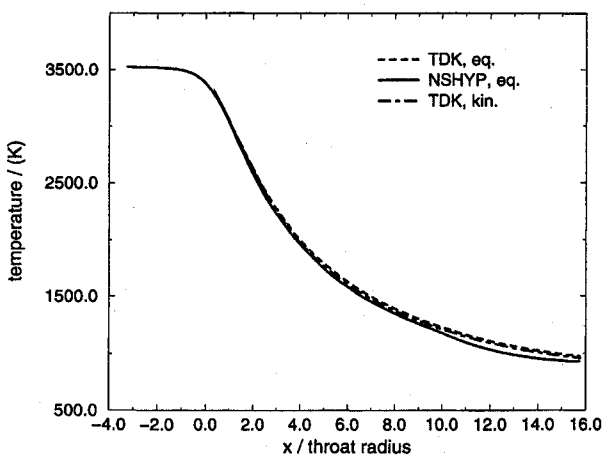

Fig. 2 Temperature on the centerline.

and chemical nonequilibrium models were used to describe the thermodynamic properties of the flow. Comparison of the presented flow data reveals good agreement of the different numerical approaches. The experimental pressure values in Fig. 4 were taken from the literature.[9] These data are slightly scattered around the numerical values, probably because of measurement uncertainties in the experiment. Furthermore, these results indicate that in high-pressure H_2-O_2 rocket engines, chemical kinetic effects have only minor influence on the rocket performance. This becomes even more clear when looking at the species mass fractions on the centerline of the nozzle, as shown in Fig. 5, obtained from TDK and NSHYP calculations. In the case of chemical equilibrium, all mass fractions continuously decrease in the flow direction, whereas the nonequilibrium values start to freeze shortly behind the nozzle throat. Since the mass fractions of the frozen dissociation products are rather low downstream of the throat area, their influence is negligible.

An adiabatic wall condition was assumed in these simulations. The influence of wall cooling on engine performance was studied previously[3] (calculations of nozzles with adiabatic and fully regeneratively cooled walls showed no differences

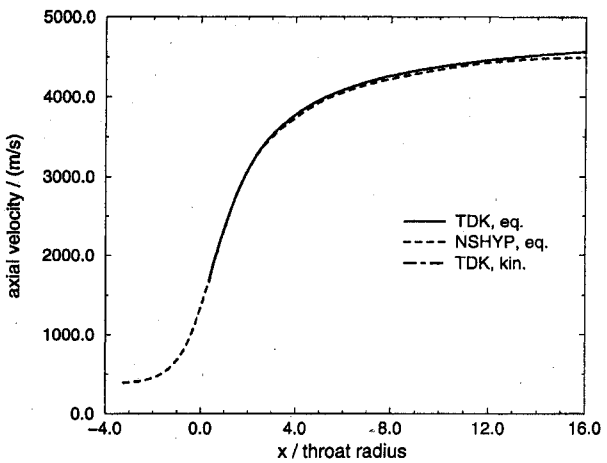

Fig. 3 Axial velocity on the centerline.

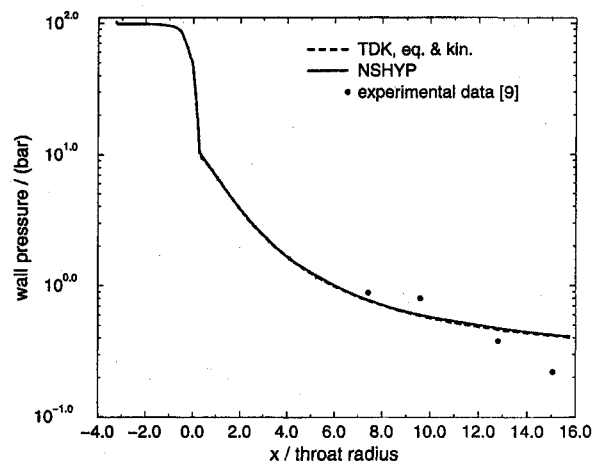

Fig. 4 Pressure values at the wall.

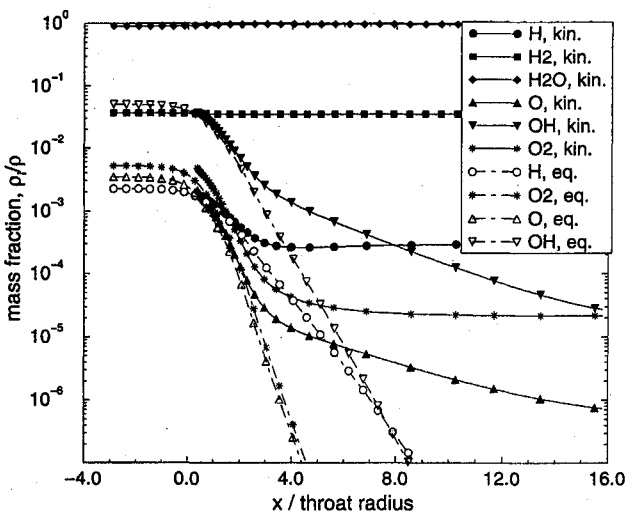

Fig. 5 Mass fractions on the centerline, r = 6.0.

Table 2 Vacuum performance parameters of the Vulcan nozzle

		$\dot{m}$, kg/s	F_{vac}, kN	I_{vac}, m/s
NSHYP	Laminar	238.4	1042.0	4369
	Turbulent	238.4	1035.5	4343
TDK	Laminar	236.1	1041.5	4412
	Turbulent	236.0	1034.1	4385

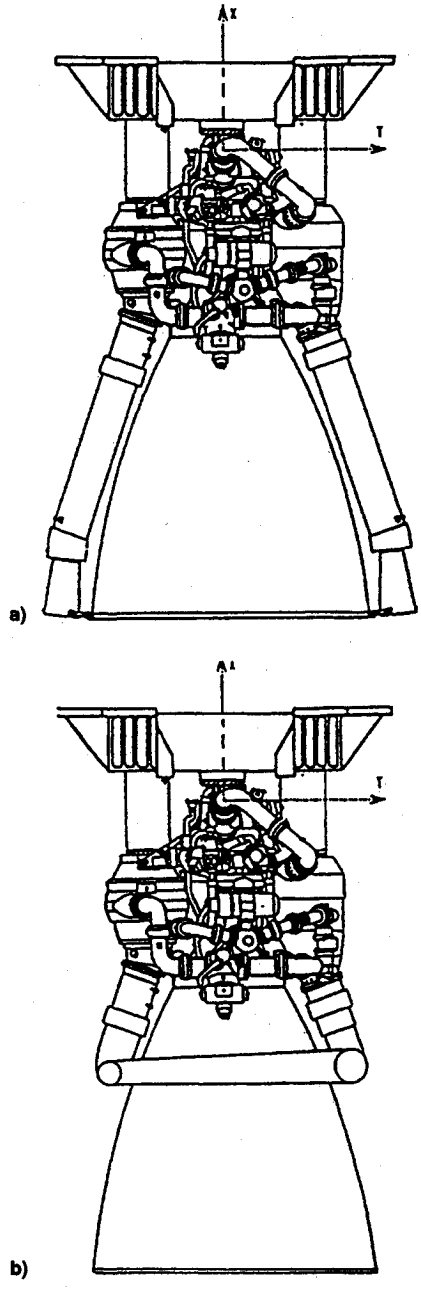

Fig. 6 a) Vulcan Mark 1 engine and b) its modified version with turbine exhaust gas injection.

in integral performance data, since the heat fluxes across the wall are transferred back to the fuel mass flow. In the case of combined regeneratively and dump cooled nozzle walls, as realized in the Vulcan engine, a decrease in performance data of ≈0.5% can be observed because of the loss of heat across the dump cooled nozzle walls[3]). Table 2 summarizes the overall performance parameters obtained by the two different simulations. Differences in integral performance data of both numerical approaches are less than 1%.

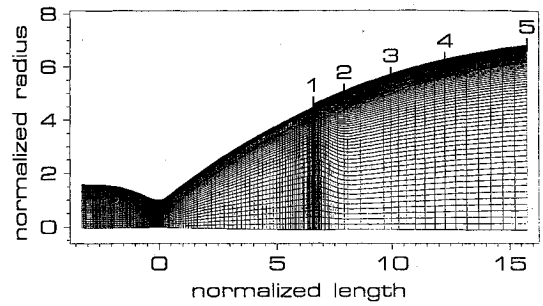

Fig. 7 (228 · 150 · 3) finite difference mesh for the modified Vulcan nozzle.

Modified Vulcan Nozzle

In the Vulcan Mark 1 engine the turbine exhaust gases of the gas-generator are ejected through small conical nozzles with low exit area ratios into ambiance. In a proposed Mark 2 version the exhaust gases are injected into the main nozzle,[6] where they are used to establish a cooling layer of the divergent nozzle contour downstream of the injection plane. Additional new design features of the Vulcan Mark 2 engine are higher chamber pressure, higher mixture ratio, a new oxygen turbopump, and some variations of geometrical data.[6]

To show the efficiency of turbine exhaust gas injection, a numerical analysis of a modified Vulcan nozzle was performed, where the turbine exhaust gases are injected into the main nozzle at an area ratio of $\varepsilon_{ar} = 20.0$. This numerical simulation is based on engine data obtained from an engine analysis of a modified Vulcan engine configuration,[7,8] where all engine design data except those of the turbine exhaust gas injection were taken from the current Vulcan Mark 1 engine design.

Figure 6 shows a sketch of the current Vulcan Mark 1 engine and its modified version. Before injection, the turbine exhaust gases are mixed with pure hydrogen that is used for dump-cooling of the divergent nozzle wall from $\varepsilon_{ar} = 5.0$ to $\varepsilon_{ar} = 20.0$ (this design of the modified engine is not equal to the current Vulcan Mark 2 design, where this dump-cooled hydrogen is injected separately at a location slightly before the turbine exhaust gas injection location). This mixture is expanded through a small toroidal nozzle and injected in the main flow direction into the main nozzle. Equal pressure values are assumed as injection criteria for minor perturbation of the main flow. Furthermore, turbine exhaust gases are injected into the main nozzle with supersonic conditions, so that any instability occurring at the injection location cannot influence the turbines. Further details concerning the engine analysis can be found in Refs. 7 and 8.

The injection area of the secondary flow results in $A_{(\varepsilon_{ar}=20.0)} = 0.0591$ m^2, which leads to a secondary nozzle exit width of approximately $\Delta r = 16$ mm. The calculation of the modified nozzle contour further downstream leads to a constant thickness of 16 mm, which must be added to the original Vulcan Mark 1 nozzle contour. Figure 7 shows a finite difference mesh of the modified nozzle, including five numbered cross sections for further evaluation. The main flow is resolved upstream of the injection cross section with 100 grid points in wall-normal direction (wall-nearest grid point at $y^+ \approx 0.1$). The injection slot with a thickness of $\Delta r = 16$ mm is resolved with 50 grid points in wall-normal direction. Downstream of the injection cross section, 150 grid points are used in wall-normal direction, again with a wall-nearest grid point at $y^+ \approx 0.1$. The main flow direction is resolved with 228 grid points. Several numerical simulations were performed to study the influence of the viscous terms in streamwise and circumferential directions (thin layer Navier–Stokes equations vs full Navier–Stokes equations). The evolution of the mixing layer near the injection location showed a slight influence, whereas integral performance data were not influenced.[8] The relevant flow data

Table 3 Injection location modified Vulcan nozzle

Area ratio main nozzle, injection	20.0
Area ratio secondary nozzle, injection	1.3
Pressure	0.877 bar
Total temperature one-dimensional, secondary flow	700 K
Temperature one-dimensional, secondary flow	457.3 K
Mach number one-dimensional, secondary flow	1.65
Mixture ratio, secondary flow	0.707

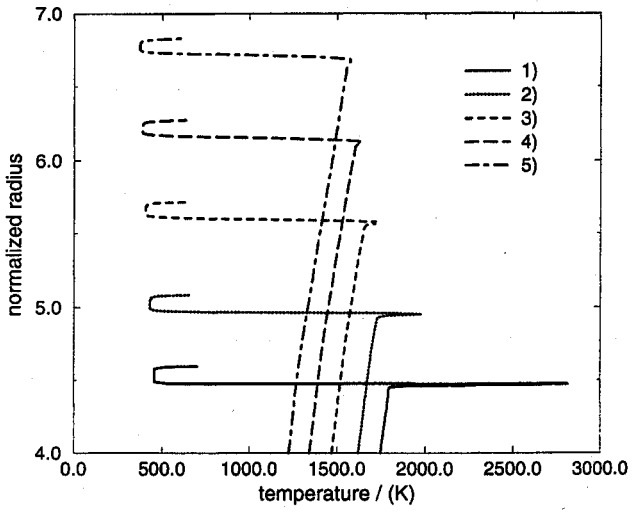

Fig. 8 Laminar temperature profiles in different cross sections in the modified Vulcan nozzle, injection section at 1) x = 6.58, 2) x = 7.9, 3) x = 10, 4) x = 12.2, and 5) x = 15.74.

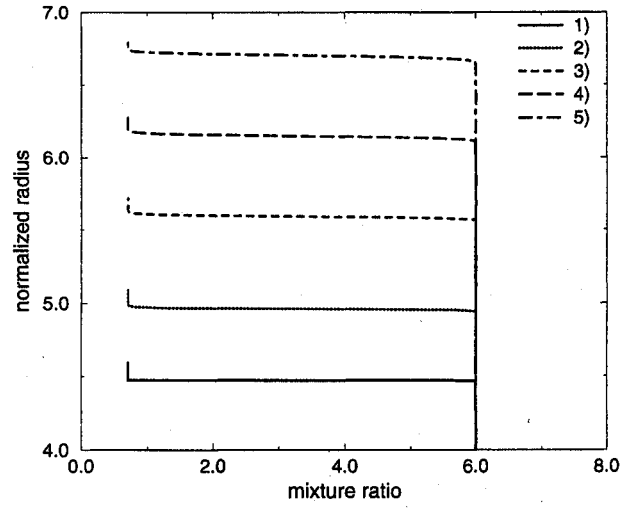

Fig. 9 Laminar mixture ratio profiles in different cross sections in the modified Vulcan nozzle, injection section at 1) x = 6.58, 2) x = 7.9, 3) x = 10, 4) x = 12.2, and 5) x = 15.74.

needed for the numerical simulation of the exhaust gas injection are summarized in Table 3.

Typical Reynolds numbers in these rocket nozzles are in the order of 10^7, calculated from chamber stagnation conditions and the nozzle throat radius. Thus, the flow will be turbulent throughout the nozzle. However, to show the influence of turbulence on the flow development, first laminar flow results will be presented. Laminar calculations of the modified Vulcan nozzle reveal no significant mixing of both mass flows. A weak mixing normal to the main flow direction in the vicinity of the shear layer can be observed, resulting in a strong decrease of main flow temperature in this zone.

A detailed view of the laminar shear flow development is given in Figs. 8 and 9, where profiles of temperature and mixture ratios are shown in different cross sections. The latter are marked in Fig. 7. The main combustion chamber mass flux and the turbine exhaust gases can be even distinguished in the nozzle exit. The profiles of the mixture ratios, shown in Fig. 9, reveal a low molecular diffusion, since diffusion velocities are an order of magnitude lower than the average flow velocities. The temperature spike in curve 1, Fig. 8, results from the adiabatic wall condition used in this numerical simulation (the spike indicates the wall of the main nozzle, this is the cross section where turbine exhaust gases are injected, see Fig. 7).

The numerical simulation of the turbulent nozzle flow attests to an intensive mixing of both mass flows downstream of the injection plane, resulting in rising gas temperature values near the wall. In addition, the growth of mixing layers leads to an increase of the mixture ratio near the nozzle wall. The strong influence of turbulent fluctuations becomes obvious by comparing the laminar flow profiles, as shown in Figs. 8 and 9, with corresponding flow profiles of the turbulent calculation, shown in Figs. 10–12.

Figure 13 shows adiabatic wall temperature of the modified Vulcan nozzle assuming laminar and turbulent flow development. Furthermore, the Vulcan Mark 1 wall temperature ob-

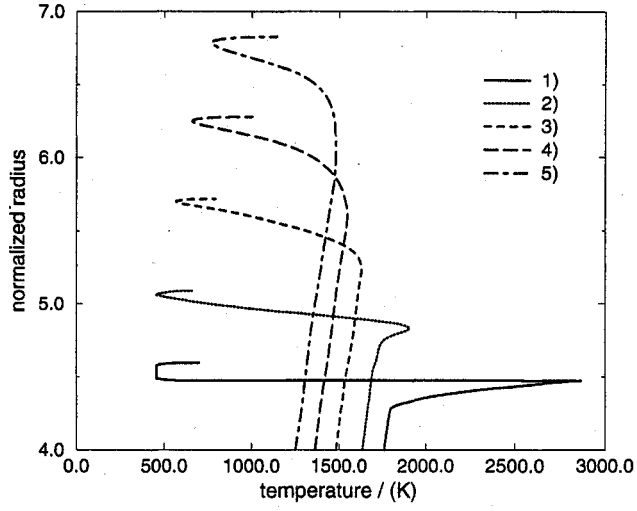

Fig. 10 Turbulent temperature profiles in different cross sections in the modified Vulcan nozzle, injection section at 1) x = 6.58, 2) x = 7.9, 3) x = 10, 4) x = 12.2, and 5) x = 15.74.

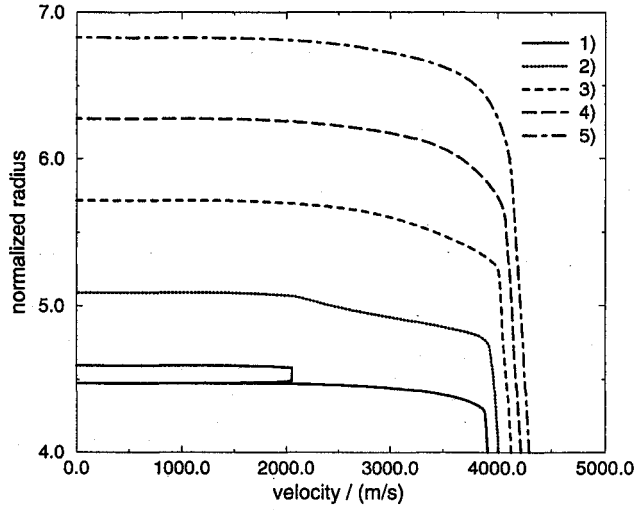

Fig. 11 Turbulent velocity profiles in different cross sections in the modified Vulcan nozzle, injection section at 1) x = 6.58, 2) x = 7.9, 3) x = 10, 4) x = 12.2, and 5) x = 15.74.

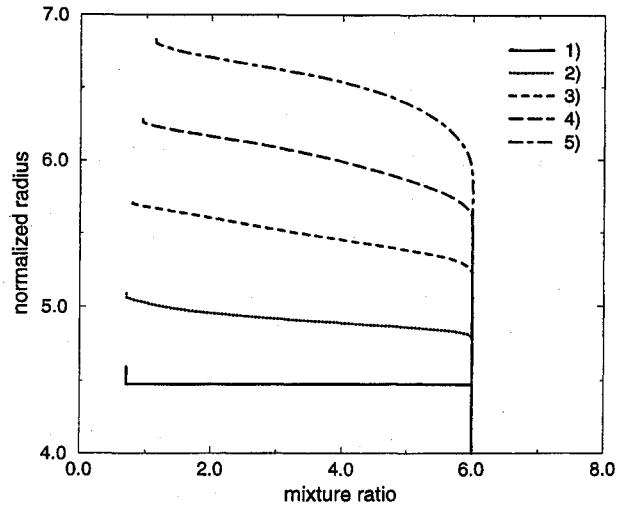

Fig. 12 Turbulent mixture ratio profiles in different cross sections in the modified Vulcan nozzle, injection section at 1) x = 6.58, 2) x = 7.9, 3) x = 10, 4) x = 12.2, and 5) x = 15.74.

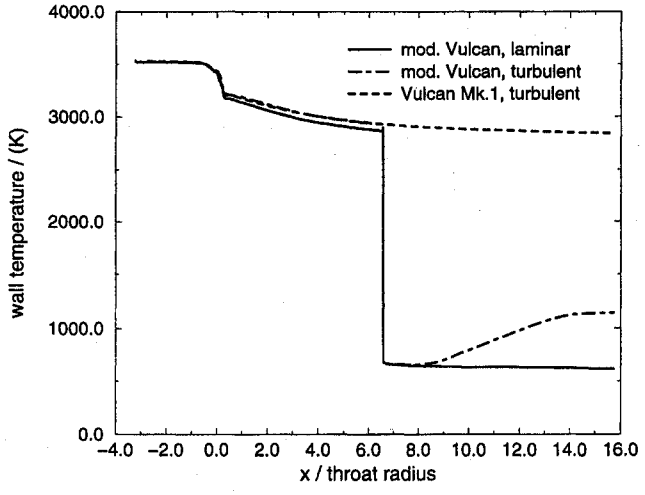

Fig. 13 Wall temperature of laminar and turbulent nozzle flow calculations.

tained from a turbulent nozzle flow calculation is also included to show the significant drop in temperature.

Corresponding effects on the skin friction coefficient are given in Fig. 14. Comparison of the laminar and turbulent solutions for the modified Vulcan calculations reveals a strong increase of the skin friction coefficient because of turbulence, inducing higher friction losses. Comparison of the turbulent solutions for both nozzles, Mark 1 and its modified version, shows the drop of the skin friction coefficient downstream the injection plane for the modified nozzle. These results indicate lower friction losses in the modified Vulcan nozzle.

Table 4 summarizes performance characteristics for both engines. The overall performance data of the Vulcan Mark 1 engine follow from the parameters for the main nozzle, given in Table 2, and performance data for the two exhaust gas nozzles, summarized in Table 5. The latter data were obtained from one-dimensional calculations assuming chemical equilibrium and an overall nozzle efficiency of $\eta_{c_F} = 0.9$ (Ref. 7).

Comparison of the specific impulse reveals a significant performance gain of the modified Vulcan engine over the Mark 1 engine for both laminar and turbulent flow. Reduced friction losses because of lower gas viscosities near the wall, caused by significantly lower mixture ratios and gas temperatures at the nozzle wall, downstream of the injection location are the main improvements obtained by the modification.

An additional numerical simulation of the modified Vulcan nozzle was performed assuming radiation cooling of the divergent nozzle wall downstream of the injection location, with an emission coefficient of $\varepsilon_r = 0.85$ for the nozzle wall. Figure 15 shows the calculated wall temperature for both, adiabatic and radiation cooled wall, with the wall temperature profile for adiabatic wall condition already shown in Fig. 13. Radiation effects lead to a slight decrease in wall temperature. However, it should be pointed out that the equilibrium chemistry as-

Table 4 Calculated performance data Vulcan Mark 1 and modified Vulcan engine

I_{vac}	Vulcan Mark 1, m/s	Modified Vulcan, m/s
Laminar	4296.4	4311.4
Turbulent	4271.4	4290.2

Table 5 Performance data Vulcan Mark 1, exhaust gas

	Turbine exhaust gas
Mass flow	9.56 kg/s
Specific impulse, vacuum	2485.3 m/s
Res. thrust	23.8 kN

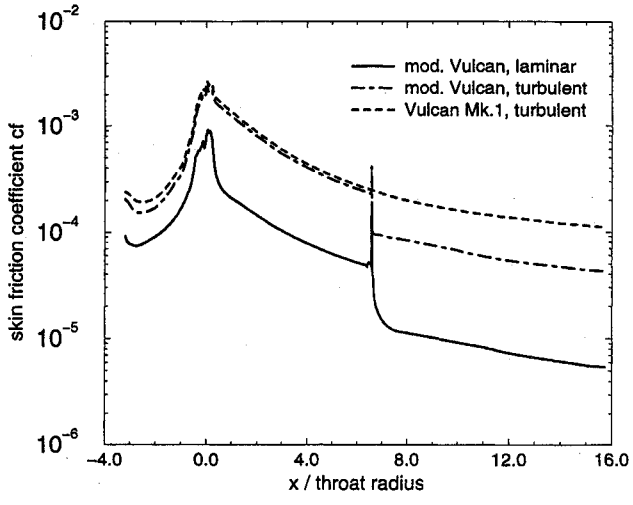

Fig. 14 Skin friction coefficient assuming laminar and turbulent flow.

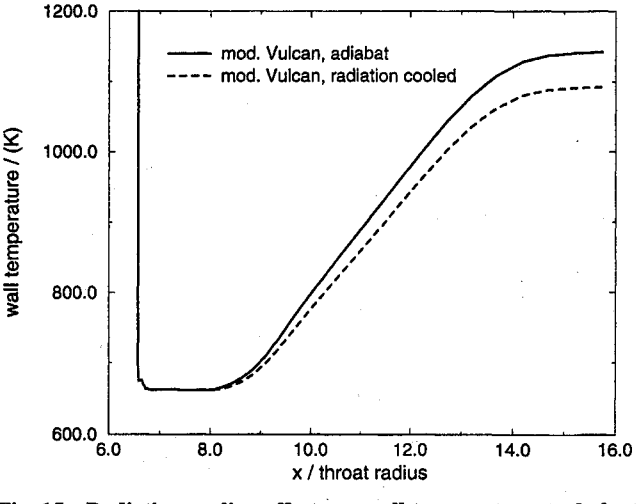

Fig. 15 Radiation cooling effects on wall temperature, turbulent flow.

sumption in the boundary layer leads to unphysically large heat fluxes or temperature drops, since heat release because of recombination is overestimated.

It is clear that adiabatic wall conditions cannot be realized in real hardware. Temperatures of the cooled nozzle walls are in the range of 600–900 K. In case of dump cooled nozzle walls as realized in the Vulcan Mark 1 engine, specific impulses of the engine will be ≈0.5% lower than in case of adiabatic or regeneratively cooled walls[3,7] (performance contribution of the dump cooling fluid is included). Thus, the performance gain for the modified version would be slightly higher than predicted within this study.

Conclusions

A numerical method has been developed for the simulation of modern rocket engine nozzle flows. The code solves the three-dimensional, time-dependent Euler and thin-layer Navier–Stokes equations in conservation-law form. Diffusion effects are included by solving two transport equations for the element mass conservation of hydrogen and oxygen, respectively.

Various simulations of a conventional, bell-type nozzle were performed for the validation of the numerical method. The comparison of the NSHYP results with the data obtained with the NASA TDK program for the Vulcan nozzle are in very good agreement.

Numerical nozzle flow simulations based on an engine cycle analysis of a modified Vulcan engine were performed. The results of these calculations indicate that an effective film cooling of the divergent nozzle part can be realized with the turbine exhaust gas injection, which dramatically reduces the adiabatic wall temperature. In addition to the lower wall temperature, reduced mixture ratios near the wall lead to an additional reduction of the friction losses. The comparison of the overall performance data for both engines, Vulcan Mark 1 and its modified version, shows a gain in overall performance values for the modified engine.

References

[1]Brenner, G., Gerhold, T., Hannemann, K., and Rues, D., "Modern Numerical Simulation of Shock/Shock and Shock-Wave/Boundary-Layer Interactions in Hypersonic Flows," *Computers and Fluids Journal*, Vol. 22, Nos. 4,5, 1993, pp. 427–439.

[2]Nickerson, G. R., Dang, L. D., and Coats, D. E., "Two-Dimensional Reference Computer Program," Marshall Space Flight Center, NAS 8-35931, Huntsville, AL, 1985.

[3]Manski, D., and Hagemann, G., "Influence of Rocket Design Parameters on Engine Nozzle Efficiencies," AIAA Paper 94-2756, June 1994.

[4]Anderson, J. D., *Modern Compressible Flow*, McGraw–Hill, New York, 1982.

[5]Hagemann, G., Hannemann, K., and Krülle, G., "Numerical Flowfield Analysis of the Next Generation Vulcan Nozzle," AIAA Paper 95-2782, July 1995.

[6]Brossel, P., and Eury, S., "Development Status of Vulcain Engine and Its Upgraded Version Vulcain Mark II," International Astronautical Federation 94-S.2.411, 1994.

[7]Goertz, C., "A Modular Method for the Analysis of Liquid Rocket Engine Cycles," AIAA Paper 95-2966, July 1995.

[8]Hagemann, G., "Supersonic Flows in Complex Nozzle Configurations of High-Performance Rocket Engines," DLR-FB 95-40, May 1996.

[9]Popp, M., "A Study of Advanced Nozzle Technologies," ELITE Program, ESTEC Noordwijk, Oct. 1993.